$(p,2p)$ reaction on ^{7}Li and ^{12}C at 100 MeV†

Ranjan K. Bhowmik,* C. C. Chang, J.-P. Didelez, and H. D. Holmgren
University of Maryland, College Park, Maryland 20742
(Received 16 June 1975; revised manuscript received 18 December 1975)

The $(p,2p)$ reaction on the target nuclei ^{7}Li and ^{12}C has been studied at 100 MeV bombarding energy. The energies of both the outgoing protons have been measured in coincidence in a coplanar symmetric geometry with good energy and momentum resolution in order to separate the different excited states of the residual nuclei. The experimental data are presented in a form suitable for direct comparison with direct knockout theory (impulse approximation). The distorted wave impulse approximation model can explain the qualitative features of the energy sharing and angular correlation spectra. The detailed quantitative agreement with the distorted wave impulse approximation is, however, somewhat poor, indicating the necessity for a more exact treatment of the three-body reaction mechanism.

[NUCLEAR REACTIONS ^{7}Li$(p,2p)$, ^{12}C$(p,2p)$, $E_p=100$ MeV; measured $\sigma(E,\theta_1,\theta_2)$; deduced distorted recoil momentum distributions; separation energy resolution 0.8 MeV; DWIA analysis.]

I. INTRODUCTION

During recent years, $(p,2p)$ experiments have become an important tool in investigating the structure of light nuclei. Most of the available experimental data can be classified into two different groups: experiments using proton energies above 150 MeV[1-9] and those below 60 MeV.[10-14] Though the first group of experiments can, in principle, give nuclear structure information directly, the energy resolution attainable at high energies was, in general, not good enough to resolve individual nuclear levels. At low energies the energy resolution was very good, but the reaction mechanism was too complicated to extract reliable nuclear structure information.

At 100 MeV bombarding energy, the $(p,2p)$ reaction is expected to be dominated by a direct knockout process. The present series of $(p,2p)$ experiments have been performed on ^{6}Li, ^{7}Li, and ^{12}C. Data have been taken with good energy and momentum resolution over a range of kinematic variables in order to study the reaction mechanism. In this paper we present a detailed experimental study of the $(p,2p)$ reaction on ^{7}Li and ^{12}C. The ^{6}Li$(p,2p)$ results have been published earlier.[15] The experimental results are discussed in Sec. II. A comparison with distorted wave impulse approximation (DWIA) calculations is presented in Sec. III to investigate the role of distortion and off-shell effects.

II. EXPERIMENT

The experimental setup has been described in a previous paper.[15] Thin (10–15 mg/cm^2) self-supporting foils of ^{12}C and isotopically enriched (99.99%) ^{7}Li were viewed by two ΔE-E counter telescopes. The experimental energy resolution for the summed energy spectrum was typically 0.8 MeV full width at half maximum (FWHM). The solid angles subtended by both detectors were 1.8 and 3.0 msr for the ^{7}Li and ^{12}C targets, respectively, resulting in a momentum resolution of 8.8 and 11.5 MeV/c for the recoil momentum spectra.[16] Data were recorded event by event on magnetic tape for off-line analysis.

Energy and momentum conservation in three-body breakup imply that

$$\vec{p}_0=\vec{p}_1+\vec{p}_2+\vec{p}_3$$

and

$$E_0=E_1+E_2+E_3+E_S ,$$

where E_0 is the kinetic energy of the incoming proton, E_1 and E_2 are the kinetic energies of the two detected protons, and E_3 is the kinetic energy of the recoiling nucleus. $\vec{p}_0$, $\vec{p}_1$, $\vec{p}_2$, and $\vec{p}_3$ are the corresponding momenta of the incoming and outgoing particles. The proton separation energy E_S is defined as $E_S=(m_p+m_{A-1}-m_A)c^2+E_x$, where m_p, m_A, and m_{A-1} are proton, target ground state, and residual nucleus ground state masses, and E_x is the excitation energy of the residual nucleus. Since $\vec{p}_1$ and $\vec{p}_2$ are measured and $\vec{p}_0$ is known, $\vec{p}_3$ and E_S are determined for each $(p,2p)$ event.

For a qualitative understanding of the reaction mechanism, the experimental data are presented in a form suitable for comparison with the first order theory of knockout reactions: viz., the plane wave impulse approximation (PWIA). In the

PWIA, the cross section is given by[17]

$$\frac{d^3\sigma}{d\Omega_1 d\Omega_2 dE_1} = (\text{PSF}) \left(\frac{d\sigma}{d\Omega}\right)_{pp} |\phi(\vec{p}_3)|^2, \qquad (2.1)$$

where (PSF) is a known three-body kinematic factor, $(d\sigma/d\Omega)_{pp}$ is the p-p scattering cross section, and $\phi(\vec{p}_3)$ is the Fourier transform of the overlap integral between the target wave function and the residual nucleus wave function. Since both PSF and $(d\sigma/d\Omega)_{pp}$ are slowly varying functions of angle and energy, the $(p, 2p)$ cross section in the PWIA is dependent mainly on the shape of $|\phi(\vec{p}_3)|^2$.

The experimental data are presented in three forms: separation energy spectra, angular correlations, and energy sharing spectra.

A. Separation energy spectra

Separation energy spectra are obtained for each angle pair by computing the recoil energy E_3 from kinematics and adding to this the energies of the two detected particles. The separation energy spectrum for the reaction $^7\text{Li}(p, 2p)^6\text{He}$ at $\theta_1 = -\theta_2 = \theta = 41°$ (angle where $p_3 \simeq 0$ for the ground state transition) and $\theta = 30°$ are shown in Fig. 1. The experimental cross sections have been averaged over the region $|E_1 - E_2| \leq 10$ MeV. The ground state and the first excited state of ^{6}He ($E_x = 1.80$ MeV) are well resolved. A smooth background is observed for $E_x = 3$ to 11 MeV. The broad bump seen in the separation energy spectra is centered about $E_x \simeq 14$ MeV. Roynette *et al.*[3] reported two

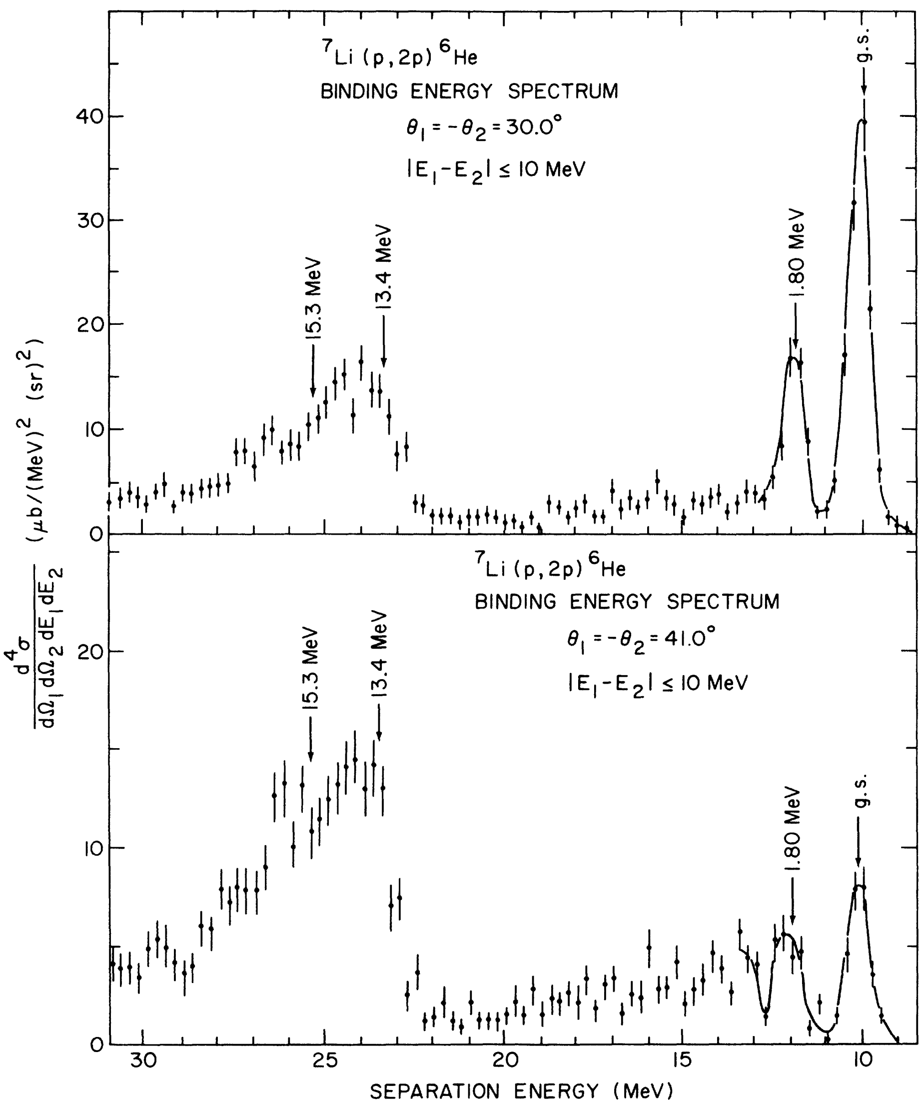

FIG. 1. Separation energy spectrum for the reaction $^7\text{Li}(p, 2p)\,^6\text{He}$ at $\theta = \theta_1 = -\theta_2 = 41°$ and $\theta = 30°$.

states of ^{6}He at 13.4 and 15.3 MeV excitation on the basis of a (p, 2p) experiment at 156 MeV. No indication of such a doublet structure is seen in the present 100 MeV data which have both better energy resolution and better statistics than the 156 MeV data. A study of the ^{7}Li(d, ^{3}He)^{6}He reaction at 80 MeV,[18] with an energy resolution of 200 keV FWHM, does not indicate any doublet structure in the excitation region corresponding to s-state knockout.

The separation energy spectrum for the reaction ^{12}C(p, 2p)^{11}B at $\theta = 28°$, averaged over the region of phase space $|E_1 - E_2| \leq 10$ MeV, is shown in Fig. 2. Figure 2 also shows all the coincident events for E_1 and $E_2 > 25$ MeV. The ground state and the 2.12 MeV state of ^{11}B are strongly excited in (p, 2p) reaction. The levels at 4.44 and 5.02 MeV are not resolved and appear as a single group with the centroid at 4.9 MeV. The peak observed at 6.8 MeV excitation is probably due to a mixture of states at 6.74, 6.79, and 7.30 MeV. A very broad bump is observed in the region of excitation E_x = 12–24 MeV, indicating the contribution from s-state knockout.

B. Angular correlation

From the two dimensional E_1 vs E_2 spectra at each angle pair, we have extracted the cross sections for the coplanar symmetric point ($\theta = \theta_1 = -\theta_2$,

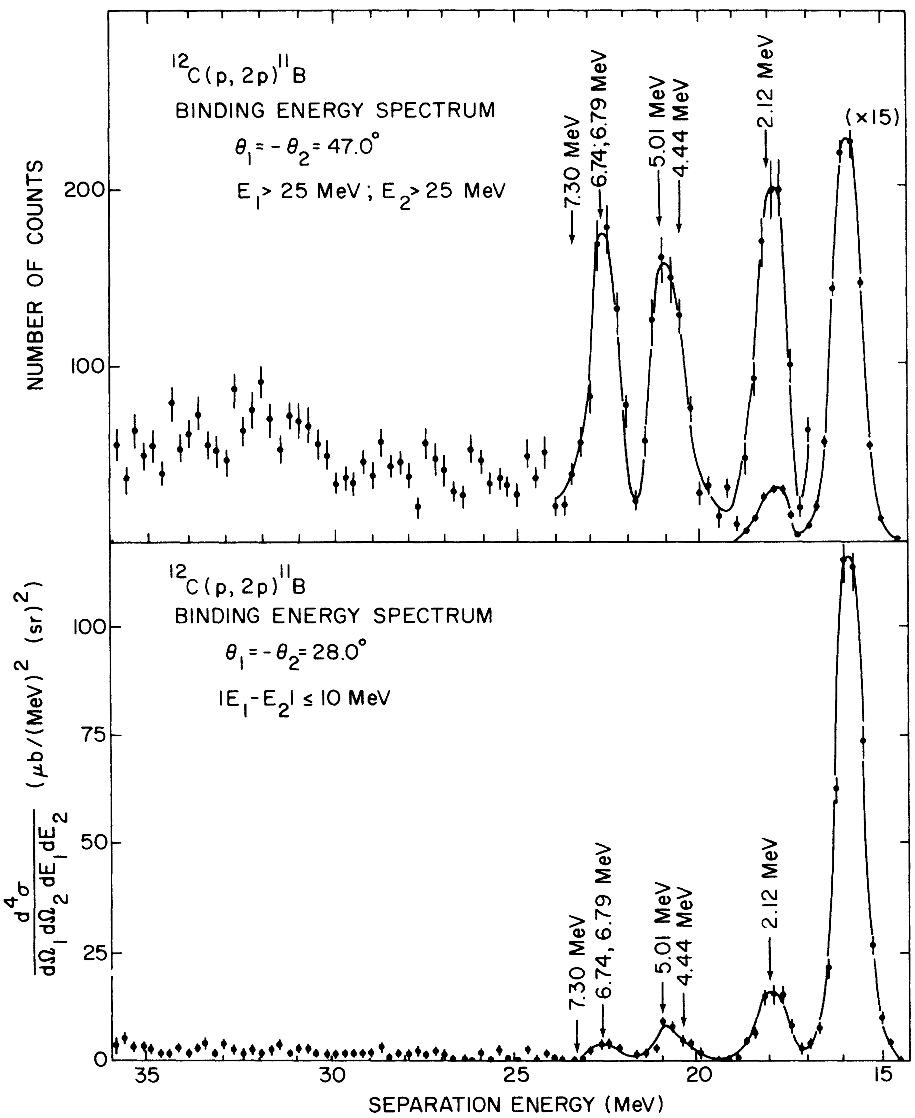

FIG. 2. Separation energy spectrum for the reaction ^{12}C(p, 2p)^{11}B at $\theta = 28°$ and $\theta = 47°$.

$E_1 = E_2$) for each state of the residual nucleus. This form of presentation of the data is commonly referred to as a coplanar symmetric angular correlation. To improve statistics the cross sections have been averaged over the region $|E_1 - E_2| \leq 10$ MeV, but the average value differs by less than 10% from the value at $E_1 = E_2$.

The angular correlation for different regions of excitation of the residual nucleus ^{6}He are shown in Fig. 3. The angular correlations for the ground state and the 1.80 MeV state are quite similar and both exhibit a deep minimum at the angle $\theta = 41°$, where p_3 can be zero.[19] The angular correlations for the regions of excitation between 11 and 25 MeV are consistent with the knockout of an s-state proton from the α core in ^{7}Li. (It is interesting to note that the angular correlation for the region of excitation between 3 and 7 MeV resembles that of the knockout of an s-state proton.)

The angular correlations for the various states in ^{11}B are shown in Fig. 4. The minimum in the ground state angular correlation occurs at $\theta \simeq 44°$, instead of at the quasifree angle $\theta = 38.5°$, where p_3 can be zero. The ratio between the small angle and large angle peaks is ~2.4/1.

The angular correlation for the 2.12 MeV state

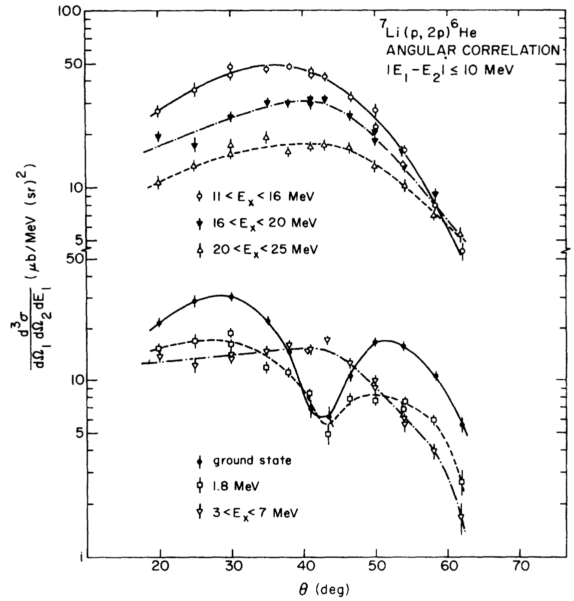

FIG. 3. Angular correlation distribution for the reaction ^{7}Li$(p, 2p)^6$He for various regions of excitation energies of the residual nucleus. The energy sharing data at each angle pair have been averaged over the region $|E_1 - E_2| \leq 10$ MeV.

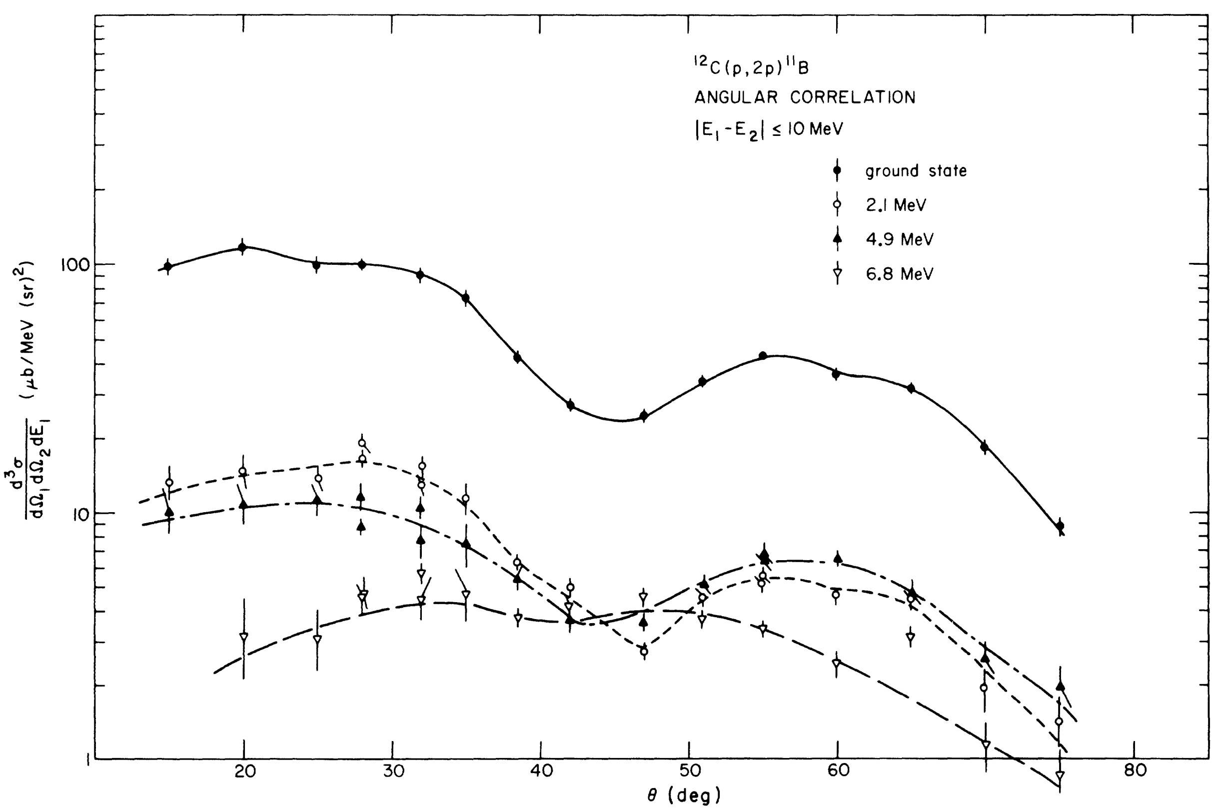

FIG. 4. Angular correlation distribution for the reaction ^{12}C$(p, 2p)^{11}$B (see Fig. 3 caption).

is quite similar to that of ground state. The angular correlation for the 4.9 MeV state is also similar, although shifted slightly towards larger angles. The ratio of the experimental cross sections at $\theta = 30°$ for these states is σ(g.s.)/σ(2.12 MeV)/σ(4.9 MeV) = 1.0/0.15/0.10. [For the ^{12}C $(d, {}^3\text{He})^{11}$B reaction at 80 MeV,[18] the ratio of the experimental cross section at the first maximum for these states is σ(g.s.)/σ(2.12)/σ(5.02) = 1.0/0.14/0.08.] The angular correlation for the 6.8 MeV state is quite different from that of the ground state. The cross section for the s-state knockout region (E_S = 28–40 MeV) is ~36 μb/MeV (sr)^2 in the angular region $\theta = 20°–45°$ and falls off for larger angles.

C. Energy sharing spectra

Energy sharing spectra are obtained by projecting the two dimensional E_1 vs E_2 spectrum for a specific separation energy region onto the E_1 axis. Due to the use of a symmetric geometry and observation of identical particles, the spectrum must be symmetric about the point $E_1 = E_2$. The recoil momentum p_3 for the residual nucleus has different values along the kinematic curve and has a minimum at $E_1 = E_2$.

In Fig. 5, the energy sharing spectra for the ground state of ^{6}He have been plotted as a function of p_3 after dividing by the kinematic factor in Eq. (2.1). For comparison, spectra for different angle pairs are presented in the same figure. (The curves are DWIA predictions and will be discussed in Sec. III B.) In the PWIA, cross section/PSF is proportional to $(d\sigma/d\Omega)_{pp} |\phi(\vec{p}_3)|^2$. Since $(d\sigma/d\Omega)_{pp}$ is a slowly varying function of E_1, the plotted quantities are essentially proportional to $|\phi(\vec{p}_3)|^2$. A marked angular dependence of the extracted momentum distribution is observed; the peak separation increases for larger θ and the distribution becomes narrower as θ decreases. A similar change in shape is also observed for the ^{12}C$(p, 2p)$-^{11}B (g.s.) reaction (Fig. 6). In this case, the maximum peak to valley ratio is observed at $\theta = 42°$, and the minimum predicted at 38.5° ($p_3 = 0$) by the PWIA is almost completely filled in.

The momentum distribution for the reaction ^{7}Li$(p, 2p)^6$He for the region of separation energy E_S 23 to 27 MeV is quite similar to the momentum distribution for s-state knockout in ^{6}Li$(p, 2p)^5$He reaction at 100 MeV. For the ^{12}C$(p, 2p)$ s-state knockout, statistics are too poor to extract any meaningful information. (This is consistent with the fact that at 100 MeV proton bombarding energy, the experimental peak cross sections for the s-state knockout region are about 230, 130, and 36 μb/MeV(sr)^2, respectively, for the ^{4}He$(p, 2p)$,[20] ^{6}Li$(p, 2p)$,[15] and ^{7}Li$(p, 2p)$ reactions.)

III. THEORETICAL ANALYSIS

In a three-body treatment of the knockout process, the reaction is assumed to take place through the mechanism

$$m_1 + (m_2 + m_3) \to m_1 + m_2 + m_3 ,$$

where m_3 refers to an inert core that remains unaffected throughout the collision process. The Hamiltonian is written as

$$H = H_0 + V_{12} + V_{13} + V_{23} ,$$

where H_0 is the free Hamiltonian for the three-particle system and V_{ij} is the interaction between

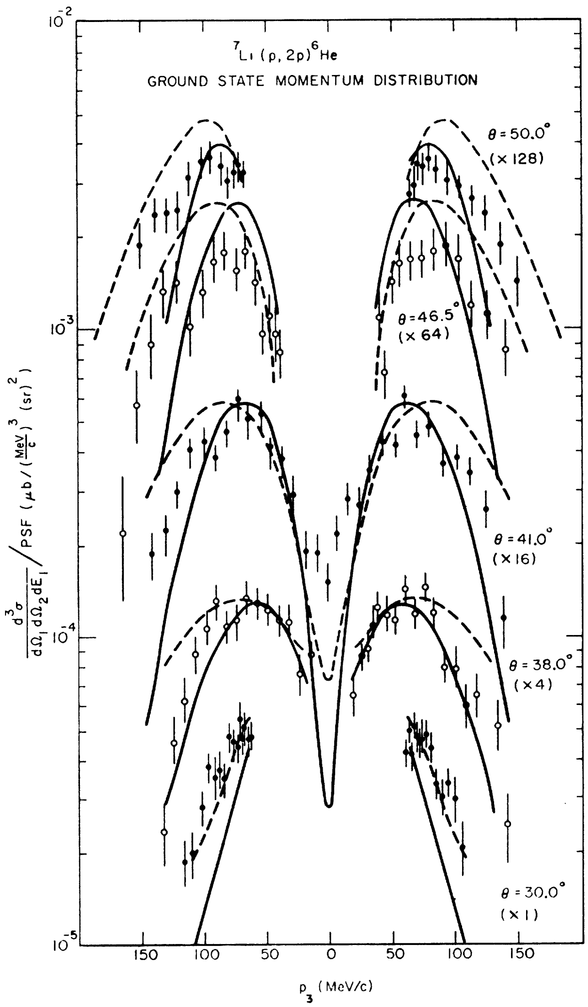

FIG. 5. Extracted momentum distribution $d^3\sigma/(d\Omega_1 d\Omega_2 dE_1)$/PSF at various angle pairs for the ^{6}He ground state. The data at each angle pair have been multiplied by the factors in the parenthesis. The theoretical curves are DWIA predictions at different angle pairs. The solid curves are for $\langle r \rangle_{rms} = 4.96$ fm and the dashed curves (---) are for $\langle r \rangle_{rms} = 3.46$ fm (see text).

the particles i and j. In the distorted wave impulse approximation (DWIA), the scattering amplitude is given by[21]

$$T_{fi} = \langle \phi_f | \Omega_f^* t_{12} \Omega_i | \phi_i \rangle \,, \qquad (3.1)$$

where Ω_i and Ω_f are Møller wave operators describing the distortion of the incoming and outgoing wave functions, respectively, in the potential $V_{13}+V_{23}$. Expanding the distorted wave functions in momentum coordinates the transition amplitude is equal to[11]

$$T_{fi} = \int\int\int\int d\vec{p}\, d\vec{p}\,'\, d\vec{p}\,''\, d\vec{p}\,'''\, \langle \vec{p}\,', \vec{p}\,'' | t_{12} | \vec{p}, \vec{p}\,''' \rangle \times \phi_{\vec{p}_1}^{(-)*}(\vec{p}\,')\, \phi_{\vec{p}_2}^{(-)*}(\vec{p}\,'')\, \phi_{\vec{p}_0}^{(+)}(\vec{p})\, \phi(\vec{p}\,''')\,, \qquad (3.2)$$

where $\phi(q)$ is the momentum wave function in the target of the knocked out proton and $\langle \vec{p}\,', \vec{p}\,'' | t_{12} | \vec{p}, \vec{p}\,''' \rangle$ are the matrix elements of t_{12} between plane wave states. In the plane wave limit

$$T_{fi}^{\mathrm{PW}} = \langle \vec{p}_1, \vec{p}_2 | t_{12} | \vec{p}_0, \vec{q} \rangle\, \phi(\vec{p}_3)\,, \qquad (3.3)$$

where

$$\vec{p}_3 = -\vec{q} = \vec{p}_0 - \vec{p}_1 - \vec{p}_2\,.$$

The t matrix, in the plane wave limit, is half off the energy shell.[22] For practical calculations in the distorted wave case, the matrix elements of t_{12} must be treated as a slowly varying function of the momentum variables so that they may be taken outside of the integral. This is equivalent to assuming a short range interaction proportional to $\delta(\vec{r}_1 - \vec{r}_2)$, where the constant of proportionality is determined by the asymptotic value of the scattering amplitude in the plane wave limit. If the t matrix is factorized outside the integral,

$$T_{fi}^{\mathrm{DW}} \simeq \langle \vec{p}_1, \vec{p}_2 | t_{12} | \vec{p}_0, \vec{q} \rangle\, \phi^{\mathrm{DW}}(\vec{p}_3)\,, \qquad (3.4)$$

where the distorted momentum distribution $\phi^{\mathrm{DW}}(\vec{p}_3)$ is given by

$$\phi^{\mathrm{DW}}(\vec{p}_3) = \int\int\int\int d\vec{p}\, d\vec{p}\,'\, d\vec{p}\,''\, d\vec{p}\,'''\, \delta(\vec{p}\,' + \vec{p}\,'' - \vec{p} - \vec{p}\,''') \times \phi_{\vec{p}_1}^{(-)*}(\vec{p}\,')\, \phi_{\vec{p}_2}^{(-)*}(\vec{p}\,'')\, \phi_{\vec{p}_0}^{(+)}(\vec{p})\, \phi(\vec{p}\,''')\,. \qquad (3.5)$$

In the DWIA, the breakup cross section is related to the distorted momentum distribution by the equation[1]

$$\frac{d^3\sigma}{d\Omega_1 d\Omega_2 dE_1} = (\mathrm{PSF})\, (d\sigma/d\Omega)_{pp} \sum_{LJ} \frac{N_{LJ}}{2L+1} \sum_M |\phi_{JLM}^{\mathrm{DW}}(\vec{p}_3)|^2\,. \qquad (3.6)$$

$(d\sigma/d\Omega)_{pp}$ is proportional to the square of the half-off-shell t matrix and corresponds to the p-p scattering cross section in the on-shell limit. N_{LJ} is the spectroscopic factor for proton removal from the target nucleus leading to a particular level of the residual nucleus.

The evaluation of the distorted momentum distribution is complicated due to the three-body nature of the final state. After separating out the equation of motion of the center of mass, the two final state particles are described by[23]

$$\left[-\frac{\hbar^2 A}{2m(A-1)}(\vec{\nabla}_{13}^2 + \vec{\nabla}_{23}^2) + V_{13} + V_{23} - \frac{\hbar^2}{m(A-1)}\vec{\nabla}_{13}\cdot\vec{\nabla}_{23}\right]\phi_f^{\mathrm{DW}}(\vec{r}_{13}\cdot\vec{r}_{23}) = E\phi_f^{\mathrm{DW}}(\vec{r}_{13}, \vec{r}_{23})\,,$$

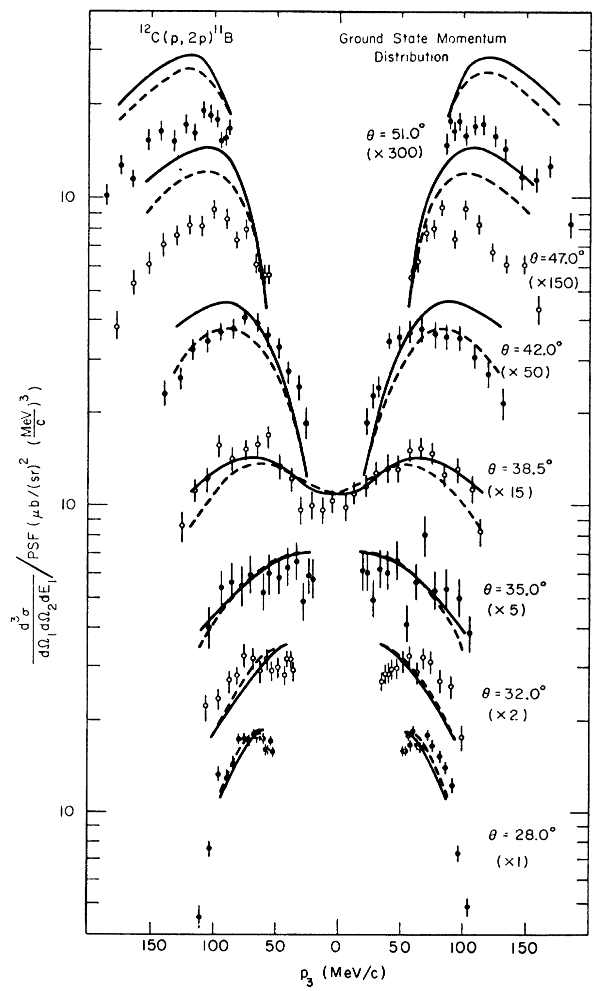

FIG. 6. Extracted momentum distributions for the ground state of ^{11}B (see Fig. 5 caption). The dashed curves (---) take into account the energy dependence of optical potentials and the solid curves (—) ignore the energy dependence.

where

$$\vec{r}_{ij} = \vec{r}_i - \vec{r}_j ,$$

$$m_1 = m_2 = m ,$$

$$m_3 = (A-1)m ,$$

and E is the total energy of the center of mass system.

If the coupling term $\vec{\nabla}_{13} \cdot \vec{\nabla}_{23}$ is ignored, the Hamiltonian is separable in the coordinates $\vec{r}_{13}$ and $\vec{r}_{23}$ and the distorted final state wave function is given by

$$\phi_f^{DW} = \chi_{\vec{k}_1}^{(-)}(\vec{r}_{13})\chi_{\vec{k}_2}^{(-)}(\vec{r}_{23})\phi(\text{core}),$$

where $\chi_{\vec{k}_i}(\vec{r})$ represent the distorted waves of asymptotic momenta[24] $\vec{k}_i = \vec{p}_i - \vec{p}_0/(A+1)$ calculated in an optical potential.

The distorted wave function of the initial state is given by

$$\phi_i^{DW} = \chi_{\vec{k}_0}^{(+)}(\vec{r}_{13} - \vec{r}_{23}/A)\,\psi(\vec{r}_{23})\phi(\text{core}),$$

where $\psi(\vec{r}_{23})$ is the single particle wave function of the knocked out proton in the target.

The distorted momentum distribution then reduces to the form[23]

$$\phi_{JLM}^{DW}(\vec{p}_3) = \frac{1}{(2\pi)^{3/2}} \int d\vec{r}\, \chi_{\vec{k}_1}^{(-)*}(\vec{r})\, \chi_{\vec{k}_2}^{(-)*}(\vec{r}) \times \chi_{\vec{k}_0}^{(+)}\left(\frac{A-1}{A}\vec{r}\right)\psi_{JLM}(\vec{r}) . \quad (3.7)$$

The half-off-shell cross sections, along with various on-shell approximations, have been calculated for Reid soft core potential[25] using the program TMAT.[26] The DWIA program WAVEPROG[27] was used to calculate the distorted momentum distributions. The overlap wave functions $\psi_{JLM}(\vec{r})$ were approximated by bound state wave functions in a Woods-Saxon potential. The well depth of the potential was adjusted to reproduce the proton separation energy E_S. The momentum distribution is found to be sensitive to the rms radius of the bound state wave function only and not to the particular combination of the geometric parameters r_0 and a of the Woods-Saxon potential.

A. Angular correlation

The theoretical angular correlation for the reaction ^{12}C(p, 2p)^{11}B(g.s.) calculated by using WAVEPROG[27] is shown in Fig. 7. The theoretical curves have been averaged over a finite energy bin $|E_1 - E_2| \leq 10$ MeV. The bound state wave function of rms radius[1] 2.98 fm was generated in a Woods-Saxon potential well with size parameters $r_0 = 1.64$ fm, $a = 0.65$ fm. Optical potentials which describe p-^{12}C scattering at 100 MeV[28] and at 40 MeV[29] (Table I) were used to compute the incoming and outgoing wave functions.[30] The spin-orbit part of the optical potentials was ignored in order to simplify the calculations. The spectroscopic factor N_{LJ} for the transition to the ground state of

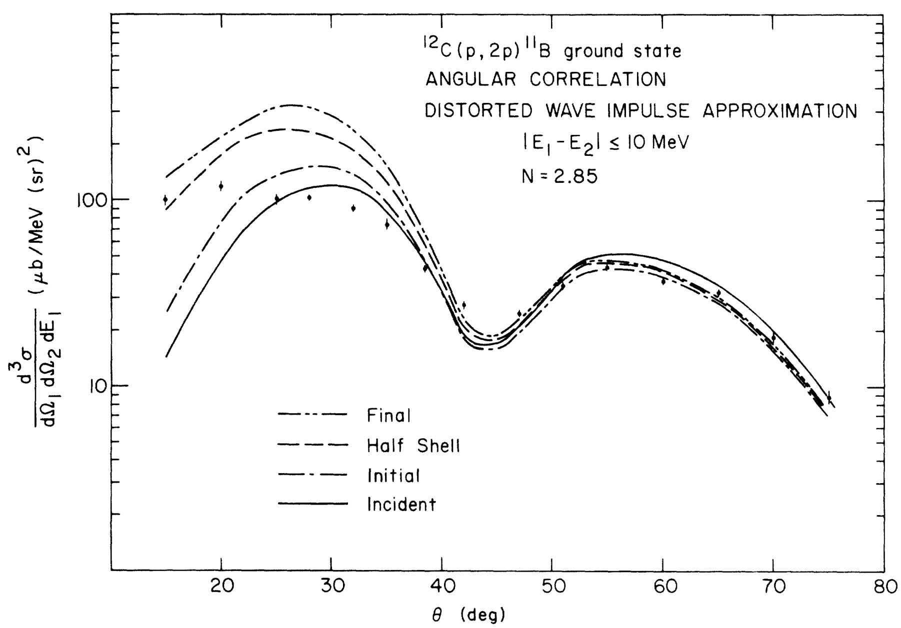

FIG. 7. Theoretical angular correlation distributions for the reaction ^{12}C(p, 2p)^{11}B(g.s.) using different prescriptions for computing $[d\sigma/d\Omega]_{pp}$ (see text).

TABLE I. Optical potentials for distorted wave calculations.

Target nucleus	Incident energy (MeV)	Potential number	Coulomb radius r_c (fm)	Real part V (MeV)	Real part r_0 (fm)	Real part a (fm)	Imaginary part W (MeV)	Imaginary part W_D (MeV)	Imaginary part r_0' (fm)	Imaginary part a' (fm)	Total Reaction Cross section σ_T (mb)	Reference number
^{7}Li	100	A_1	1.83	20.83	1.226	0.69	...	10.54	0.84	0.62	204	28
		A_2	1.83	17.84	1.39	0.63	20.94	...	1.11	0.52	199	28
^{6}Li	50	B_1	1.20	37.8	1.14	0.79	...	4.48	1.32	0.48	188	33
		B_2	1.20	32.9	1.09	0.80	0.24	2.08	1.50	0.39	102	33
		B_3	1.20	34.3	1.17	0.59	4.75	...	2.00	0.66	306	33
^{12}C	100	C_1	1.33	21.59	1.296	0.508	...	5.39	1.396	0.52	273	28
		C_2	1.33	22.61	1.255	0.55	4.37	...	1.908	0.21	260	28
^{12}C	40	D_1	1.25	43.8	1.15	0.65	...	7.58	1.25	0.38	324	29
		D_2	1.25	38.6	1.15	0.73	7.15	...	1.25	0.44	251	29
		D_3	1.25	41.5	1.15	0.66	...	5.01	1.10	0.52	274	29
		D_4	1.25	37.5	1.15	0.66	4.29	...	1.25	0.82	240	29
		D_5	1.25	35.2	1.15	0.67	5.03	...	1.10	0.85	226	29
		D_6	1.25	47.2	1.07	0.65	6.60	0.81	1.25	0.75	372	29

^{11}B was taken to be 2.85 (Ref. 31). The dashed curve is for the half shell prescription; the dot-dashed and dot-dot-dashed curves are for on-shell approximations by using "initial energy" and "final energy" prescriptions. The full curve ("incident") was obtained by assuming $(d\sigma/d\Omega)_{pp}$ to be a constant, having a value corresponding to the incident proton energy of 100 MeV.

The angular correlation for $\theta > 50°$ is fitted fairly well in absolute magnitude in all four prescriptions. The shift of the minimum of the angular correlation towards large angles and the broadening of the large angle peak are due to refraction effects in the nuclear optical potential. At forward angles, all four prescriptions, i.e., half shell, initial energy, final energy, and incident energy, fail to fit the angular correlation. To investigate which factor may contribute to the breakdown of the DWIA, we have studied the sensitivity of DWIA calculations to the optical potential parameters, the bound state wave function, and refraction effects on the t matrix.

For light nuclei optical model parameters are not very well defined and various sets of optical potentials are available that give reasonably good fits to the elastic scattering data. We have studied the effect of the ambiguity of optical potentials on the distorted momentum distribution by using various pairs of potential combinations listed in Table I. The distorted momentum distributions were found to be quite independent of the optical potentials used for the incoming channel. The choice of optical potential for the outgoing channels affected the absolute magnitude but the qualitative shape (i.e., the ratio of the maxima at forward and backward angles) did not change (Fig. 8). The magnitude of $|\phi^{\mathrm{DW}}|^2$ depends critically on σ_R (see Fig. 8 and Table I). To investigate whether the use of ^{12}C parameters for the residual nucleus ^{11}B affects the distorted momentum distribution, we have allowed the real and imaginary well depths for the outgoing particle potential to vary, keeping the geometrical parameters fixed. The increase in V shifted the minimum in the angular distribution towards larger angles and the increase in W or W_D caused an overall attenuation and a filling of the minimum. Varying V, W, or W_D by ±25% did not change the ratio of the two maxima at forward and backward angles by more than 10%.

At 50 MeV bombarding energy, the DWIA and DWTA[32] (distorted wave t matrix approximation) results are strongly affected by a change in the final state optical parameters and are relatively insensitive to the bound state wave function. On the other hand, at 100 MeV and higher incident energies the bound state wave function is reasonably well determined from the large angle angular

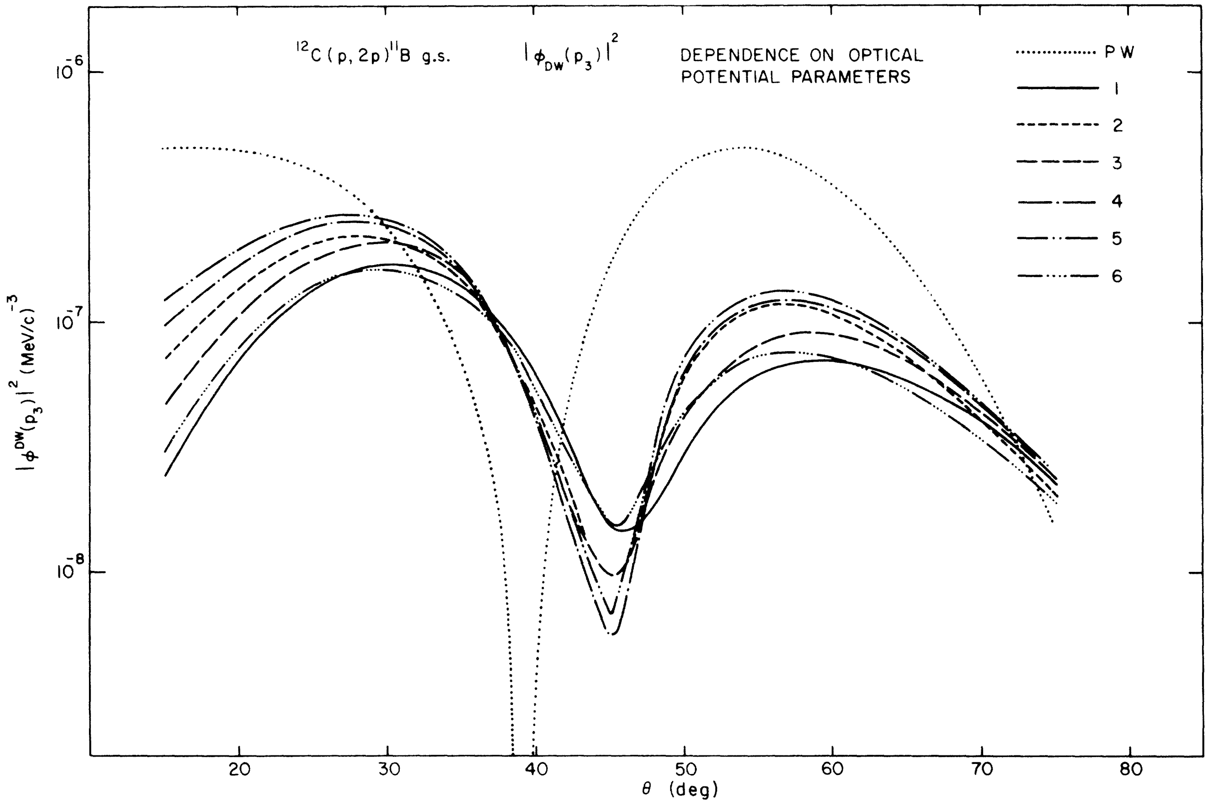

FIG. 8. Distorted momentum distributions $|\phi_{JL}^{DW}(p_3)|^2$ for the reaction ^{12}C(p, 2p)^{11}B (g.s.). The six curves are for the incoming potential C_1 and outgoing potentials ($D_1 - D_6$). PW is the plane wave momentum distribution with the optical potentials set to zero.

correlation data. The ratio of the distorted momentum distribution at forward and backward angles is almost independent of the bound state wave function parameters.

The above considerations indicate that the shape of the distorted momentum distribution is fairly well fixed in the DWIA; i.e., it is insensitive to reasonable changes in the bound state and optical model parameters. On the other hand, the p-p cross section in Eq. (3.6) is sensitively dependent on the choice of the off-shell extrapolation process, as can be seen in Fig. 7. The half-off-shell prescription gives the cross section in the zero distortion limit and predicts a rapidly rising cross section for forward angles. In the strong absorption limit the momenta of the incoming and outgoing protons would be increased due to refraction in the nuclear potential, and $(d\sigma/d\Omega)_{pp}$ would tend to approach a constant value. The ratio of cross sections at the small angle and at the large angle peaks for a p-state distribution would therefore depend critically on three-body effects in the quasifree scattering process.

For the reaction ^{7}Li(p, 2p)^{6}He, the comparison of experimental angular correlation with DWIA is shown in Fig. 9. The wave function parameters are taken from Ref. 1 ($\langle r \rangle_{\rm rms} = 4.96$ fm). The distorted momentum distributions have been averaged over the kinematic region $|E_1 - E_2| \leq 10$ MeV. Optical potentials obtained from p-^{7}Li scattering at 100 MeV[28] and p-^{6}Li scattering at 50 MeV[33] were used to compute the incoming and outgoing distorted waves. The theoretical fit to the angular correlation is found to be relatively poor in all four prescriptions. The theoretical cross section decreases much faster with θ than the experimental data, and the experimental spectroscopic factor $N_{LJ} = 0.067$ is much smaller than the value of 0.6 predicted by shell model calculations.[31] The experimental spectroscopic factor is, however, quite sensitive to the bound state wave function used. A reduction of the size parameters of the bound state potential well to $r_0 = 2.25$ fm, $a = 0.65$ fm, $\langle r \rangle_{\rm rms} = 3.46$ fm increases the spectroscopic factor to $N_{LJ} \simeq 0.24$ and improves the fit to the angular correlation (Fig. 9). The fit is quite good for $\theta > 50°$ and the fit for small angles is also somewhat improved.

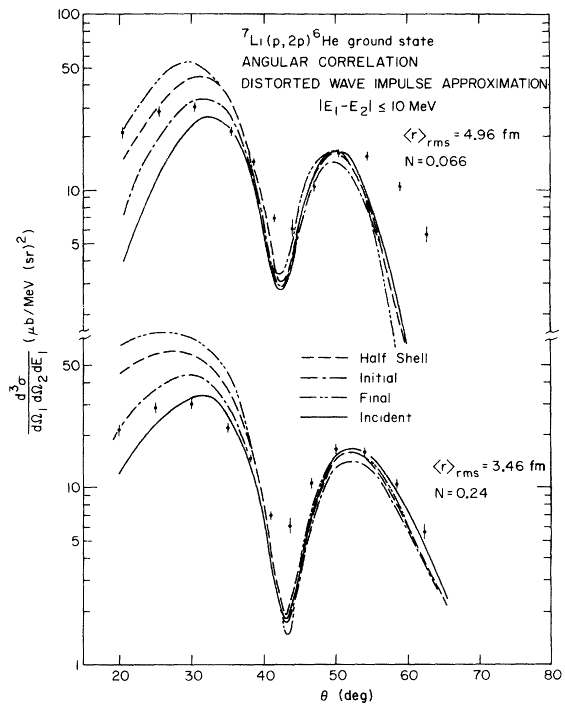

FIG. 9. Theoretical angular correlation distributions for the reaction ^{7}Li(p, 2p)^{6}He(g.s.) using different prescriptions for calculating $[d\sigma/d\Omega]_{pp}$. The two sets of curves are for two different bound state wave functions for the ^{6}He.

B. Energy sharing spectra

In a coplanar symmetric geometry, the shapes of the energy sharing spectra are determined mainly by distortion effects and are relatively insensitive to the choice of prescription used to calculate $(d\sigma/d\Omega)_{pp}$. In Fig. 5, $(d\sigma/d\Omega)_{pp}$ has been taken to be a constant (i.e., incident energy prescription), and the experimental cross sections at different angle pairs are compared with the DWIA. The two sets of curves correspond to the two different bound state wave functions for ^{7}Li used in Fig. 9. The theoretical curves have been normalized to the experimental data at $\theta = 41.0°$. The change in shape as the angle increases is also consistent with the DWIA calculations. The ratios of peak cross sections at different angle pairs are approximately reproduced in the incident energy prescription.

In the case of the ^{12}C(p, 2p)^{11}B reaction we have studied the effect of the energy dependence of the optical potential for the outgoing particles. A linear dependence of the form

$$V(E) = V(E_A) + \frac{dV}{dE}(E - E_A),$$

$$W(E) = W(E_A) + \frac{dW}{dE}(E - E_A)$$

was used. V and W are the real and imaginary part of the optical potential, and E_A is the average energy of the outgoing protons. The geometrical parameters are held constant. The dashed curves in Fig. 6 are obtained by assuming $dV/dE = -0.3$[34] and $dW/dE = 0$. The full curves correspond to $dV/dE = dW/dE = 0$. The momentum distributions for $dV/dE = -0.3$, $dW/dE = -0.1$ are indistinguishable from the dashed curves. Thus the qualitative features of the distorted momentum distributions are not changed when the energy dependence is taken into account. Distortion nicely explains the filling-in of the expected minimum at $\theta = 38.5°$ (angle where P_3 can be zero) and the deep minimum observed at $\theta = 42°$.

IV. SUMMARY AND CONCLUSIONS

We have studied the (p, 2p) reaction at 100 MeV on ^{7}Li and ^{12}C. The experimental resolution achieved in this experiment has been good enough to resolve individual states in the residual nuclei. Data have been taken over a wide region of phase space for a detailed comparison with theory.

The overall agreement of the DWIA with the experimental data is reasonably good. The main problem is due to the failure to predict the ratio of maxima in the angular distribution at forward and backward angles. This ratio is strongly dependent on the off-shell effects in the t matrix. A fully off-shell version for the t matrix has recently been proposed,[35] but quantitative results are not yet available. Other possible sources of discrepancies are due to the neglect of spin-orbit terms in the optical potential and the coupling term $\vec{\nabla}_{13} \cdot \vec{\nabla}_{23}$ in the final state Hamiltonian. In the plane wave limit, the effect of the coupling term is included in DWIA; an exact treatment of the coupling term is, however, beyond the scope of DWIA and would require solving the three-body Schrödinger equation for the final state. Such work is presently underway[36] with the hope of a more thorough understanding of nucleon knockout reactions.

We wish to express our indebtedness to Dr. P. G. Roos for many interesting discussions, Dr. N. S. Chant for assisting us and for the use of his DWIA code, and Dr. E. F. Redish for providing us with the computer code for calculating off-shell p-p scattering cross sections. We wish to thank also Dr. N. R. Yoder for his assistance with the data acquisition on-line program and the entire staff of the University of Maryland cyclotron for the operation of the cyclotron. Finally, the use of the facilities of the Computer Science Center of the University of Maryland is acknowledged.

†Work supported in part by the U.S. Energy Research and Development Administration.

*Present address: Michigan State University, East Lansing, Michigan 48824.

[1]H. Tyren, S. Kullander, O. Sundberg, R. Ramachandran, P. Isacsson, and T. Berggren, Nucl. Phys. 79, 321 (1966).

[2]I. A. MacKenzie, S. K. Mark, and Tseh Y. Li, Nucl. Phys. A195, 609 (1972).

[3]J. C. Roynette, M. Arditi, J. C. Jackmart, F. Mazloum, M. Riou, and C. Ruhla, Nucl. Phys. A95, 545 (1967).

[4]G. Tibell, O. Sundberg, and R. O. Renberg, Ark. Fys. 25, 433 (1963).

[5]B. Gottschalk, K. H. Wang, and K. Strauch, Nucl. Phys. A90, 83 (1967).

[6]A. N. James, P. T. Andrews, P. Butler, N. Cohen, and B. G. Lowe, Nucl. Phys. A133, 89 (1969).

[7]S. Kullander, G. Lemeilleur, P. U. Renberg, G. Landaud, J. Yonnet, B. Fagerstrom, A. Johansson, and G. Tibell, Nucl. Phys. A173, 357 (1971).

[8]W. D. Simpson, J. L. Friedes, H. Palevsky, R. J. Sutter, G. W. Bennett, B. Gottschalk, G. Igo, R. L. Stearns, N. S. Wall, D. M. Corley, and G. C. Phillips, Nucl. Phys. A140, 201 (1970).

[9]T. Yuasa, and E. Hourany, Nucl. Phys. A103, 577 (1967); E. Hourany, T. Yuasa, J. P. Didelez, M. Hage Ali, F. Reide, and T. Takenchi, Nucl. Phys. A162, 624 (1971).

[10]C. A. Miller, D. I. Bonbright, J. W. Watson, and F. J. Wilson, in *Proceedings of the International Conference on Few Particle Problems in Nuclear Interactions, Los Angeles, California, 1972,* edited by Ivo Šlaus, S. A. Moszkowski, R. P. Haddock, and W. T. H. van Oers (North-Holland, Amsterdam, 1973), p. 731.

[11]H. G. Pugh, D. L. Hendrie, M. Chabre, E. Boschitz, and I. E. McCarthy, Phys. Rev. 155, 1054 (1967).

[12]L. C. Welch, C. C. Chang, H. Forster, C. Kim, D. Devins, and P. Deutchman, Nucl. Phys. A158, 644 (1970).

[13]R. M. Eisberg, D. Ingham, M. Makino, C. Kim, and C. Waddell, Nucl. Phys. A175, 58 (1971).

[14]K. Richie, R. Eisberg, M. Makino, and C. Waddell, Nucl. Phys. A131, 501 (1969).

[15]R. K. Bhowmik, C. C. Chang, P. G. Roos, and H. D. Holmgren, Nucl. Phys. A226, 365 (1974).

[16]The momentum resolutions were calculated by the program MOMRATH using the known solid angles and energy resolution of the detectors. For a given geometry, the recoil momentum distribution $W(p)$ is approximately Gaussian in shape, with a width depending on target studies. The folded momentum distribution is given by $|\phi^{\rm FOLD}(p_3)|^2 = \int |\phi(p)|^2 W(p)\,dp$.

[17]G. Jacob and Th. A. J. Maris, Rev. Mod. Phys. 38, 121 (1966).

[18]J.-P. Didelez, C. C. Chang, R. Bhowmik, H. D. Holmgren, R. I. Steinberg, and J. Wu, Bull. Am. Phys. Soc. 19, 1022 (1974).

[19]The minimum is less pronounced for the 1.80 MeV state, part of which may be accounted for by a contamination from the continuum background.

[20]H. G. Pugh, P. G. Roos, A. A. Cowley, V. K. C. Cheng, and R. Woody, Phys. Lett. 46B, 192 (1973).

[21]L. R. Dodd and K. R. Greider, Phys. Rev. 146, 675 (1966).

[22]E. F. Redish, G. J. Stephenson, and G. M. Lerner, Phys. Rev. C 2, 1665 (1970).

[23]D. F. Jackson and T. Berggren, Nucl. Phys. 62, 353 (1965).

[24]$\vec{k}_i$ are the momenta of the particles 0, 1, and 2 in the three-body center of mass.

[25]R. V. Reid, Ann. Phys. (N.Y.) 50, 411 (1968).

[26]E. F. Redish (private communication).

[27]N. S. Chant (private communication).

[28]T. Y. Li and S. K. Mark, Can. J. Phys. 46, 2645 (1968).

[29]J. A. Fannon, E. J. Burge, D. A. Smith, and N. K. Ganguly, Nucl. Phys. A97, 263 (1967).

[30]The optical potentials used in calculating the distorted momentum distributions in Fig. 5–9 are (A_1, B_1) and (C_1, D_1) for ^{7}Li(p, $2p$)^{6}He and ^{12}C(p, $2p$)^{11}B unless otherwise specified.

[31]S. Cohen and D. Kurath, Nucl. Phys. A101, 1 (1967).

[32]K. L. Lim and I. E. McCarthy, Nucl. Phys. 88, 433 (1966).

[33]G. S. Mani, D. Jacques, and A. D. B. Dix, Nucl. Phys. A165, 145 (1971).

[34]B. A. Watson, P. P. Singh, and R. E. Segel, Phys. Rev. 182, 977 (1969); K. H. Bray, M. Jain, K. S. Jayaraman, G. Lobianco, G. A. Moss, W. T. H. van Oers, D. O. Wells, and F. Petrovich, Nucl. Phys. A189, 35 (1972).

[35]E. F. Redish, Phys. Rev. Lett. 31, 617 (1973).

[36]S. K. Young and E. F. Redish, University of Maryland Technical Report No. 74-014, 1974 (unpublished).